Marine and Petroleum Geology 167 (2024) 107003

Contents lists available at ScienceDirect

Marine and Petroleum Geology

journal homepage: www.elsevier.com/locate/marpetgeo

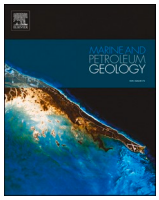

Provenance composition and evolution of marine black shales in the Yangtze platform from Ediacaran to Silurian

Xiaoqi Wang [a,*], Mingliang Wang [a], Derek Elsworth [b], TianTian Xu [a]

[a] Key Laboratory of Mine Water Resource Utilization of Anhui Higher Education Institute, School of Resources and Civil Engineering, Suzhou University, Suzhou, 234000, China

[b] John and Willie Leone Family Department of Energy and Mineral Engineering, EMS Energy Institute and G3 Center, Pennsylvania State University, University Park, PA, 16802, USA

ARTICLE INFO

Keywords:
Yangtze platform
Trace elements
Provenance analysis
Black shale

ABSTRACT

Provenance is important in understanding the evolution of geological structure and the coupling of the basin-mountain system. Although many geochemical data document the three sets of marine black shales (Ediacaran to Silurian) in the Yangtze Platform, the evolution characteristics of their sediment sources remain unclear. We gather a huge database from 307 published papers totaling 12,342 analyzed samples to establish provenance. Pearson correlation coefficient and multivariate statistical analyses were performed to establish the element and mineral links in the black shale. Nine immobile elemental ratios (Ti/Th, Th/Sc, Cr/Th, Ti/Zr, Sc/Ta, Ti/Nb, Sc/La, Zr/Sc, and La/Ti) were employed to indicate provenance. The results show that the black shales of the Longmaxi and Niutitang formations are relatively enriched in redox sensitive and productivity related elements such as V, Cr, Mo, U, Co, Ni, Cu, Zn, and Ba. The use of provenance analysis proxies, including V, Cr, Mo, Ce, Fe, P, Ba, Cu, Ni, and Si, should be approached with caution due to the potential interference of marine authigenic components. The three black shales have provenance compositions that gradually extend from intermediate to felsic from the Doushantuo to the Niutitang to the Longmaxi shale. This difference in provenance is a response to the Pan-African and Kwangsian orogenic structures which are likely to impact the paleomarine environment by variable biotrophic element inputs.

1. Introduction

Marine black shales are widely distributed in the Yangtze region in the Doushantuo, Niutitang, and Longmaxi formations, which are high-quality source rocks and are the most prospective targets for marine shale gas exploration and development in China. These shales were deposited in the Ediacaran to early Paleozoic during the convergence and accretion orogeny of Gondwana (Ren and Wang, 2023), recording the geological information of the Pan-African and Kwangsian movements. Extensive research has been conducted on the sedimentary paleo-marine environment and organic matter accumulation mechanisms of these three sets of black marine shale. These studies have accumulated a huge volume of data on the element geochemistry of black shales — however, provenance analysis of these shales has not yielded a definitive picture. For each shale, there is a debate about whether the sedimentary provenance is an intermediate or felsic igneous source (Zhang et al., 2021; Li et al., 2022; Xiao et al., 2020, 2021; Zhou et al., 2021; Ding et al., 2023). Most element testing studies fail to discuss provenance, resulting in the underutilization of these data. In most cases, the terrigenous detrital composition is a superimposed response of multiple tectonic activities. However, a systematic deconstruction of the provenance of black shales during the Ediacaran to early Paleozoic periods remains elusive. This limits our understanding of geological structure evolution and the coupling of the basin-mountain system of South China.

The elemental geochemistry of the shales contains crucial geological information about rock composition, weathering and transport processes, sedimentary environment, and diagenetic processes (Fralick and Kronberg, 1997). A crucial aspect of element-based provenance analysis is in evaluating the efficacy of employed proxies. However, it is uncertain whether current geochemical proxies, which are primarily based on turbidites or graywackes (Bhatia, 1983; Mclennan, 1993; Bhatia and Crook, 1986), are applicable in the case of black shale polymetallic enrichment. Marine black shales are highly enriched in productivity and

* Corresponding author.
E-mail addresses: 1030086301@qq.com, TB17010016B2@cumt.edu.cn (X. Wang).

https://doi.org/10.1016/j.marpetgeo.2024.107003
Received 26 March 2024; Received in revised form 5 July 2024; Accepted 10 July 2024
Available online 14 July 2024

redox-sensitive elements such as Si, P, V, Ni, Cu, Co, and Cr (Yan et al., 2021; Ye et al., 2022; Chen et al., 2016; Xiao et al., 2020). These elements may not be primarily derived from terrigenous inputs, but have been frequently used as proxies for provenance or paleoclimate (the weathering perspective of terrestrial rocks) (Ding et al., 2023; Li et al., 2019; Yan et al., 2019; Zan et al., 2021; Han et al., 2022; Xiao et al., 2021). The reliability of these provenance proxies needs to be further confirmed through statistical analysis of a large dataset.

Here, we compile element content data from published observations and analyses for these three sets of black shales to evaluate provenance and tectonic history of the Yangtze block during the Pan-African construction period. We identify the composition characteristics of terrestrial elements, infer the tectonic background of the source area, and then combine the findings of detrital mineral chronology to explain how sediments respond to the tectonic evolution of the Yangtze region.

2. Geological background

The Yangtze Platform is the main continental block in East Asia. The Paleoproterozoic and Archean crystalline basements are currently the earliest known remnants of the continental crust of the Yangtze block (Jiao et al., 2009). In the Tonian, there was significant tectonic activity on the western and northern margin of the Yangtze block with a widely distributed subduction accretion complex and arc magmatic belt (Hu et al., 2020). The Yangtze block merged with the Cathaysia block via the Jiangnan Orogen, forming the South China block (SCB) during the early Neoproterozoic (850–820 Ma) (Zhang et al., 2013; Shu, 2020). Shortly after the collision, a regional extension formed the Nanhua Rift Basin, creating significant space to accommodate the middle to upper Neoproterozoic successions (Shu, 2020; Zhang et al., 2013). The infilled formation included, in ascending order, siliciclastic sediments and bi-modal igneous (Tonian), tillite with inter-glacial clastic rocks (Cryogenian), then Doushantuo black shale covered by carbonatite (Ediacaran) (Xue et al., 2021; Wang et al., 2010). The Pan-African movement that occurred during the E-C transition resulted in significant orogenic movements in Gondwana and its periphery (Ren and Wang, 2023). However, less magmatic activity is apparent in the Yangtze Block during this period (Wang et al., 2022). Affected by global sea level rise, the Early Cambrian formed phosphate and black shale (Niutitang Formation and equivalents) deposits (Li et al., 2019). Subsequently, until the

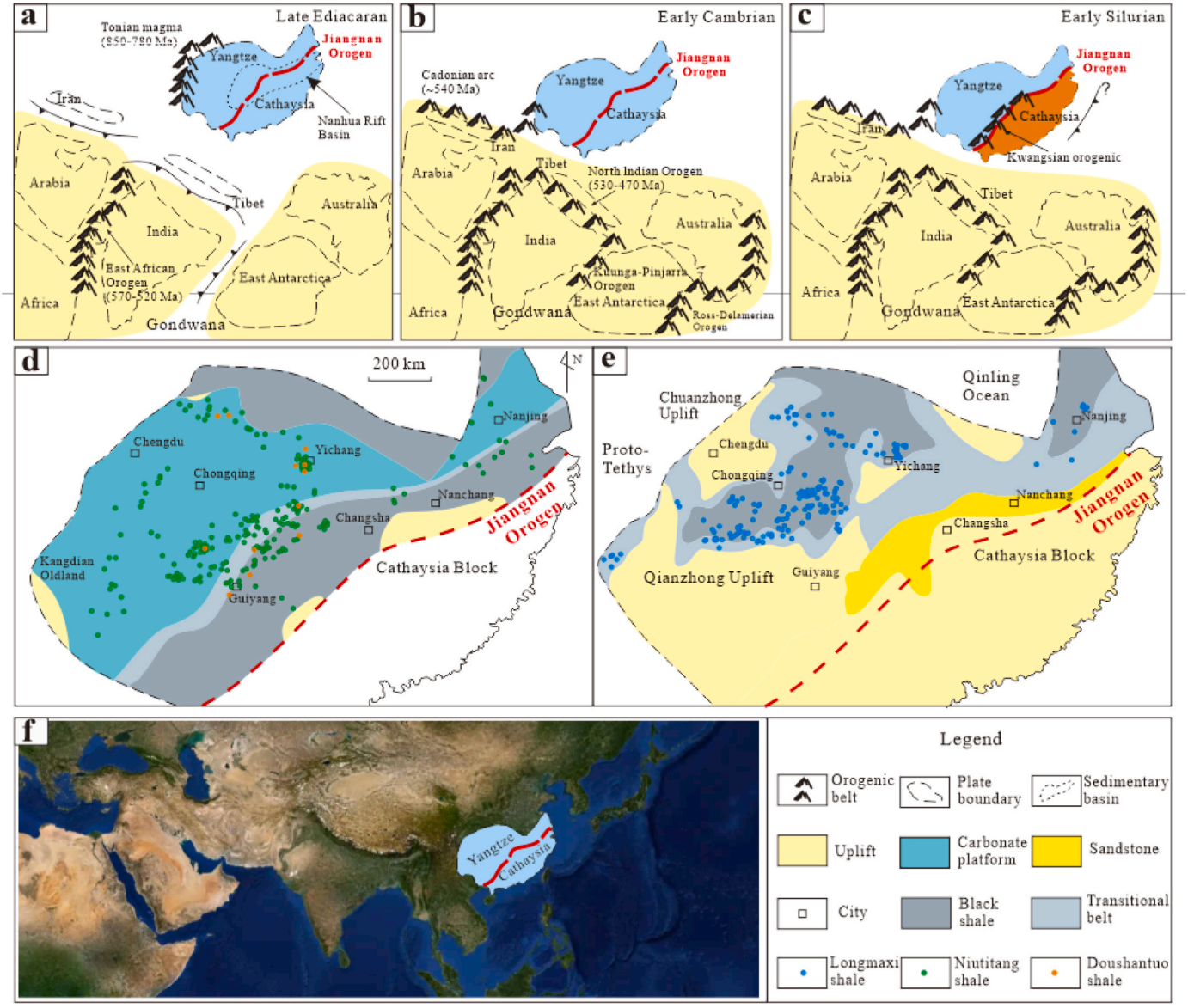

Fig. 1. Simplified palaeogeographic map of the Yangtze Platform during the E-C transition (a, b, d modified from Steiner et al. (2001); Yao et al. (2022) and O–S transition (c,e modified from Lu et al. (2021)) showing the geological setting and the distribution of dataset locations.

Middle Ordovician, it inherited the geographical characteristics of the Ediacaran period, with lithofacies distributed from west to east as tidal flat and carbonate platform sedimentation. The presence of detrital zircons from the Pan-African movement in the Cambrian of the Yangtze Block suggests its close relationship with Gondwana. The first Phanerozoic tectonic event of the SCB occurred during the Ordovician-Silurian – the Kwangsian Movement, which led to large-scale crustal folding, magmatism, and metamorphism in the eastern part of the SCB, forming the foreland basin on the Yangtze Platform (Yao and Li, 2016; Shu, 2020). Against the backdrop of global sea level rise at the Ordovician-Silurian transition, the Yangtze Block hosted the deposition of the Longmaxi black shale (Zan et al., 2021).

3. Methods

We compile a database of black shale elemental contents, comprising 307 papers quantifying the Longmaxi, Niutitang, and Doushantuo formations (see supplemental data and references). The total number of analyzed samples is 12,342. The palaeogeographic map and the distribution of datasets are shown in Fig. 1. The database for the Longmaxi shale consists of 198 elemental geochemical datasets in units of the sampled profile or well from 145 references. The Niutitang shale contains 219 datasets from 154 references. These two shale formations have been studied the most intensively and thus have accumulated the most preliminary data. The Doushantuo shale database comprises 13 datasets from 10 references. Even though the dataset is smaller than the first two, it still contains 468 samples.

The Enrichment Factor (EF) serves as a widely utilized indicator for characterizing the enrichment of an element in comparison to its average concentration in the upper continental crust (UCC). For any given element X, its enrichment factor, denoted as X-EF, can be calculated using the formula $[(X/Al)_{sample}/(X/Al)_{UCC}]$, where $(X/Al)_{sample}$ and $(X/Al)_{UCC}$ represent the weight content ratio of element X to Al in samples and UCC, respectively. However certain pitfalls accompany this approach when aluminum content is minimal. Here, we directly represent the enrichment of elements by the element content ratio of the sample to average upper continental crust abundance. This ratio directly gives the actual enrichment degree of elements without considering the effects of variable Al content from provenance. Any value larger than unity represents the enrichment of an element relative to its average upper crustal abundance.

The analytical chemical data are presented in closed form for most major, minor, and trace elements. Consequently, as the concentration of certain elements increases, there is an inverse relationship with the concentration of others. This leads to correlation measurements and graphical representations that do not accurately reflect the true underlying relationship. Here, we used the centered log-ratio transformation to remove these closure effects (Aitchison, 1982). The Principal Component Analysis (PCA) and the Pearson Correlation Coefficient (PCC) were utilized to establish element-mineral links using "factoMineR" and "factoextra" packages (Lê et al., 2008; Kassambara, 2017; Ravidà et al., 2023) and the "cor" function in R. The details of these approaches are described in Caracciolo et al. (2012, 2023).

4. Results and discussion

4.1. Geochemistry and chemical-mineral affinities

As shown in Fig. 2, the black shale of the Longmaxi and Niutitang Formations are relatively enriched in V, Cr, Mo, U, Co, Ni, Cu, Zn, and Ba, relative to the Earth's upper crust. The Doushantuo Formation has lower contents of these elements and is only significantly enriched in Mo

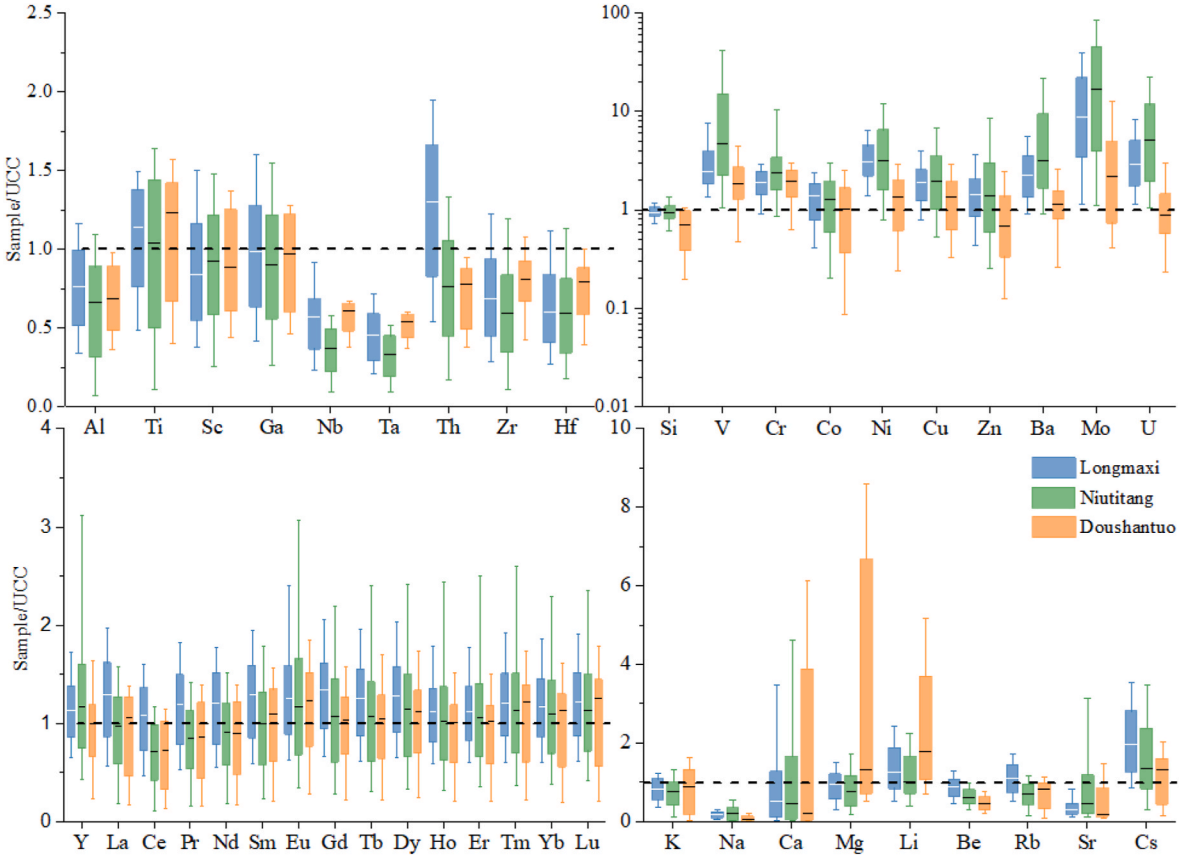

Fig. 2. Box-and-whisker plots showing standardized shale element content using the average composition of the Earth's upper crust (Taylor and Mclennan, 1985). a. Immobile elements under epigenetic conditions. b. Redox and productivity sensitive elements. c. Rare-earth elements. d. Other elements.

and V. The three sets of black shale have similar contents of Ti, Sc, Ga, K, Rb, and rare-earth elements (REE) and lower contents of Si, Al, Nb, Ta, Na, Be, Sr, Zr, and Hf to that in the Earth's upper crust. The content of Ca, Mg, Li, and Sr vary over a large range. The Longmaxi Formation has a prominently higher Th content.

As shown in Fig. 3, Al, K, Ti, Sc, Cr, Th, Zr, and La are positively correlated (>50%, most >60 %) with each other in all three types of black shales. The PCC scores for V, Mo, U, Ni, Cu, and Zn exceed 50% in the Longmaxi and Niutitang shale. However, in Doushantuo shale, this positive correlation is only observed between V, Mo, and U. Ca, Mg, and Sr produce conspicuously negative PCC scores with Si. For the Doushantuo shale, the elements negatively related to Ca, Mg, and Sr extend to Al, K, Ti, Sc, Cr, Th, Zr, and La.

The outcomes of principal component analysis are illustrated in Fig. 4 and 5. The Scree-plot of principal component analysis (Fig. 4) shows that the distribution of explained variances is consistent across all three shales for the first ten principal components. The first principal component (PC1) is associated with the elements Al, K, Ti, Sc, Cr, Th, Zr, and La and accounts for 35%–40% of the total variance. The second principal component (PC2) is linked to Ni, Cu, and Zn and represents 18%–20% of the total variance. These two principal components show similar patterns in three sets of shales. From the third principal component onwards, there are variations in the types of major contributing elements. The first five principal components collectively explain approximately 80% of the total variance in these shales.

K-means clustering separated the variables into five geometrical cluster centroids. The results are slightly different between the three shales. We first extracted the common parts of similar clusters in these shales and sorted them into five groups (Table 1). Group 1 includes Zr, Th, Cr, La, and Sc. The former three of these are almost exclusively linked with a small number of heavy minerals (Craigie, 2018). This group is therefore thought to be associated with heavy minerals. Group 2 consists of Al, K, and Ti. The former two elements are associated with clay minerals, attributed to the larger proportion of clay in shale. It is worth noting that many samples contained neither Nb nor Ta among the data we collected. To enhance the scope of data for PCC and PCA analyses, these two elements were omitted from both methods. Based on a separate correlation analyses, Nb and Ta exhibit strong correlations with Ti, Al, etc., thus they are categorized into Group 2. Both PCC and PCA analysis indicate that elements in Group 1 and Group 2 are strongly associated with each other suggesting that these elements are concentrated in the clay-size fraction resulting from a grain-size effect. Group 3 contains Mo, U, and V, all of which are widely used as paleo-redox proxies since their autogenetic inputs are controlled by redox

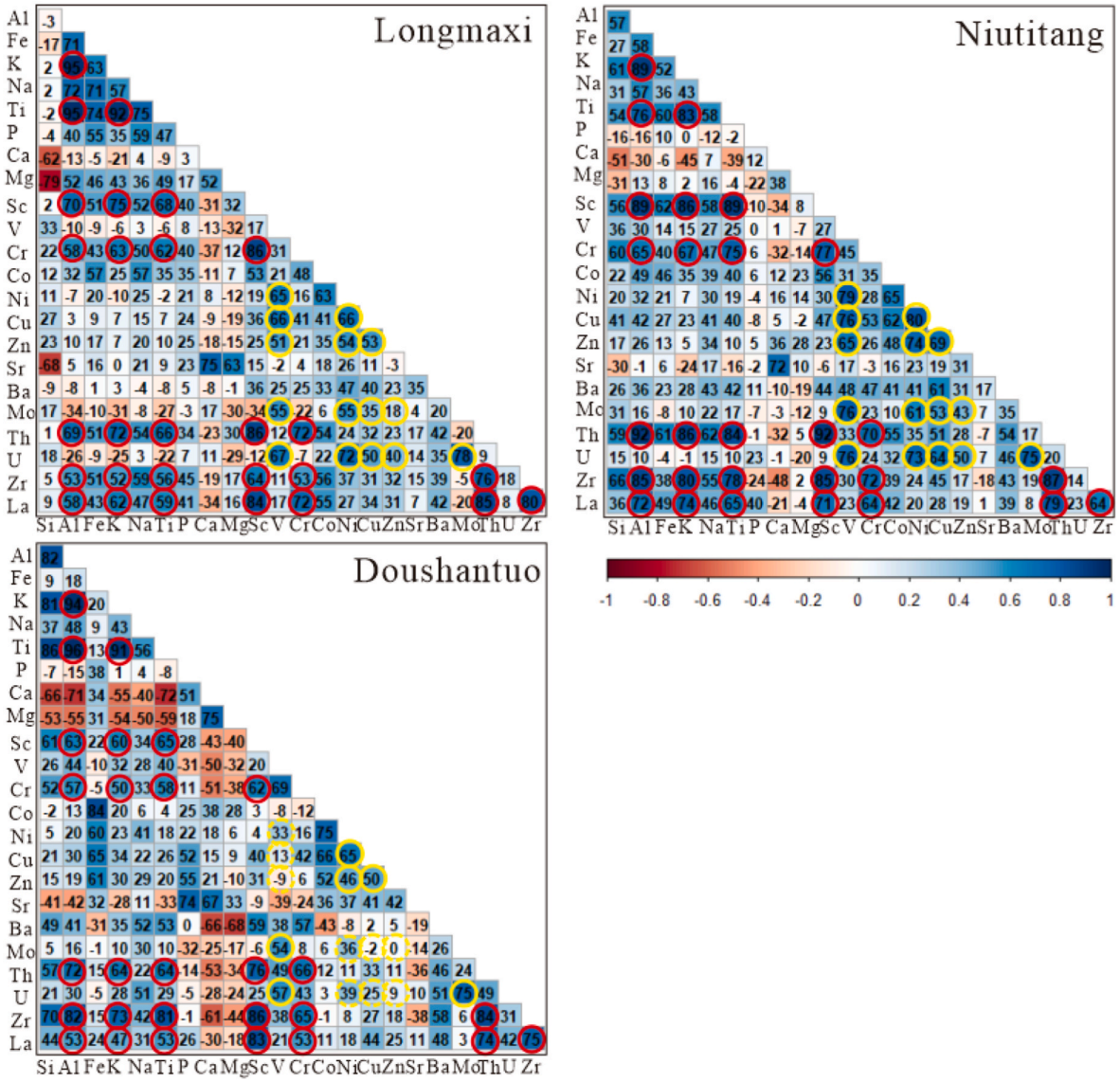

Fig. 3. Pearson correlation matrix of the element content transformed by the centered log-ratio method.

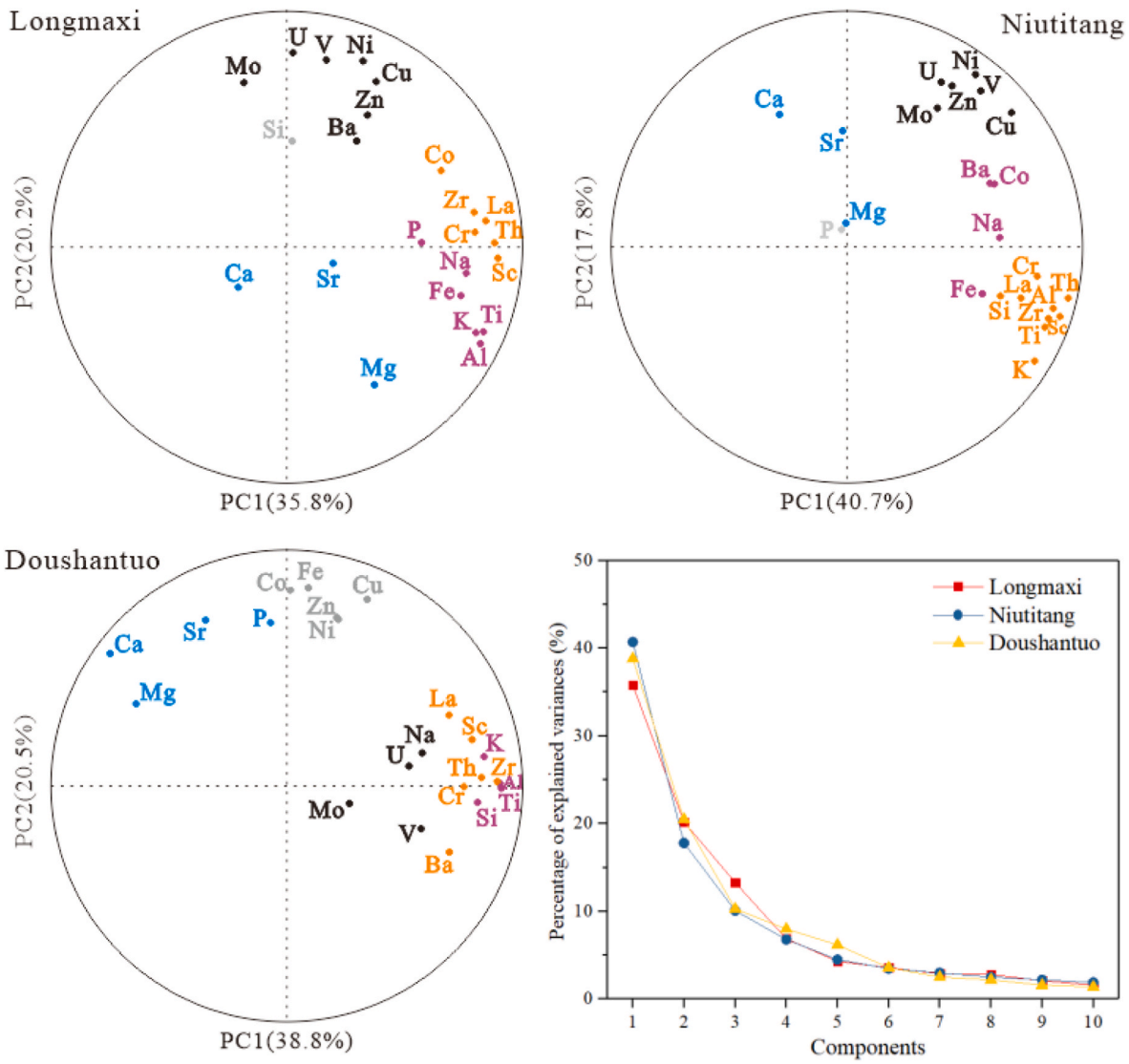

Fig. 4. Principal component load diagram and scree-plot.

conditions. Group 4 contains Ni, Cu, and Zn. Similar to Group 3, these elements are also enriched in anoxic environments. These two groups are divided into one cluster by K-means clustering in the Longmaxi and Niutitang shale. In the case of Doushantuo shales, Ni, Cu, and Zn may be related to Fe-oxyhydroxides-related authigenic minerals. Group 5 consists of Ca, Mg, and Sr, all of which may primarily be present in carbonate minerals attributed to the inversely or uncorrelated with Si and Al. The distribution of other elements varies across different clusters of shales. In the Longmaxi shale, Si is segregated into a cluster and shows a closer affinity with groups 3 and 4, which represent the autogenic components. This suggests a potential association with biosilicon input. Conversely, in other shales, Si is categorized into groups 1 and 2, representing clastic inputs. The situation for Ba is similar to that for Si. P is divided into terrigenous groups in the Longmaxi shales, a single cluster in the Niutitang shales, and the carbonate group in the Doushantuo shales. Fe and Co are divided into autogenetic components in the Doushantuo shales and terrigenous components in other shales.

4.2. Inheritance of provenance information

Provenance analysis is commonly evaluated based on elemental proxies but, despite their frequency of use, most of these proxies have received little comparative evaluation or assessment of their applicability to paleomarine systems of black shale. The elemental composition of sediments reflects geological information such as source rock, weathering, transportation, sedimentation, diagenesis, and potential hydrothermal alteration and metamorphism (Fralick and Kronberg, 1997). Before conducting source analysis, it is necessary to determine whether the proxies inherit the characteristics of the source rock material composition and are unaffected by later sedimentation or metamorphism.

There are currently a variety of plots available for provenance analysis. Most of these plots are based on data from turbidites and sandstones, and some of them contain autogenetic elements sensitive to oxidation-reduction, paleoproductivity and carbonate deposit from Groups 3 to 6 showed in Table 1. These elements may include Mo, U, V, P, Cu, Ni, Zn, Ca, Mg, Ba, Fe, Si among others. This directly impacts the accuracy of using the above elements for provenance analysis. Table 2 shows the affected plots, including many of those commonly used.

We also examined sedimentary sorting and recycling using the Zr/Sc–Th/Sc plot (Mclennan, 1993) prior to provenance analysis. The ratio Zr/Sc represents the enrichment of zircon where Zr is strongly enriched, while Th/Sc is a sensitive indicator of igneous provenance composition. As shown in Fig. 6, none of the three sets of shales have significant enrichments of zircon (high Zr/Sc ratio), discounting any influence from sedimentary sorting and recycling. These shales follow the

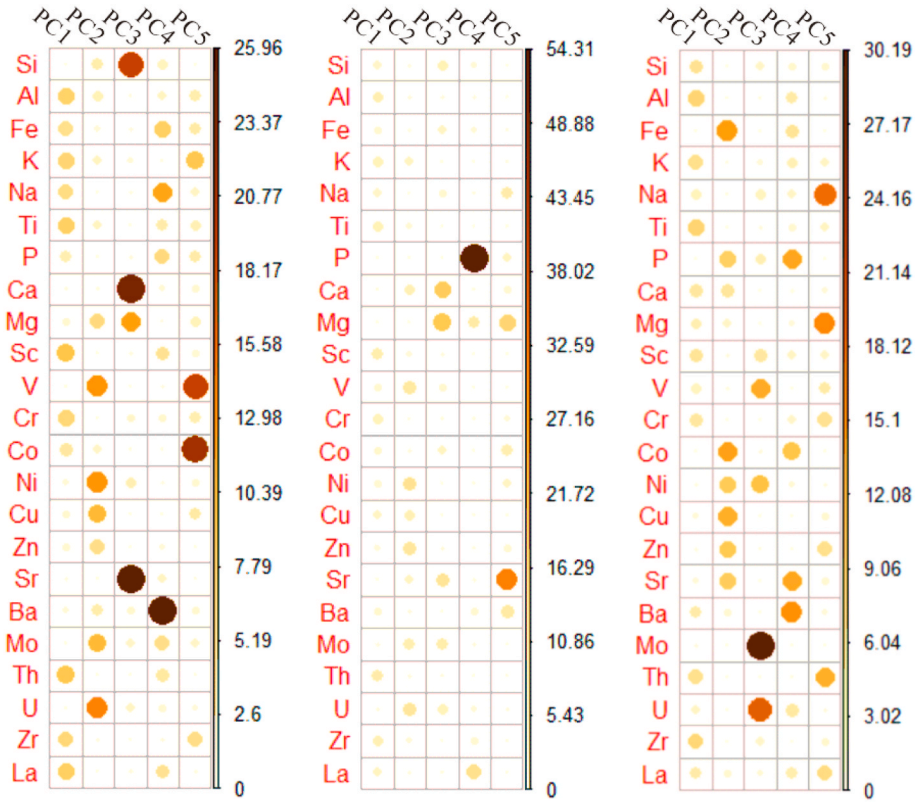

Fig. 5. Incidence of variables to the top five principal component.

Table 1
Summary of Element and Mineral Links in black shale.

Group 1	Heavy minerals
Zr	Zircon
Th	Monazite, zircon and apatite
Cr	Chrome spinel and other heavy minerals
La	Monazite, clay minerals and feldspars
Sc	Zircon, garnet, clay minerals and feldspars
Group 2	**Clay minerals and Ti-related heavy minerals**
Al	Clay minerals
K	Clay minerals (especially illite)
Ti	Titanomagnetite, magnetite, ilmenite, brookite, rutile, anatase, and/or
Ta	sphene
Nb	
Group 3	**Autogenic input influenced by paleoredox**
Mo	Pyrite, Fe-oxyhydroxides, carbonate and/or clay minerals
U	Organic matter with redox influence
V	Adsorbed onto clay minerals in anoxic conditions
Group 4	**Autogenic input influenced by paleoredox**
Ni	Pyrite, Fe-oxyhydroxides, carbonate and/or clay minerals
Cu	
Zn	
Group 5	**Carbonate minerals**
Ca	Calcite, Dolomite
Mg	Dolomite
Sr	Calcite, Dolomite
Group 6	**Various mineralogical affinity in different shales**
Co	Pyrite, Fe-oxyhydroxides, carbonate and/or clay minerals
Ba	Potassium feldspar, biotite and biogenic baryte
P	Biogenic phosphate, apatite and monazite, carbonate and clay minerals.
Fe	Haematite, magnetite, goethite, ilmenite, pyrite, clay and carbonate minerals.
Si	Mainly quartz, but part of any silicate mineral

Table 2
Commonly used plots for provenance analysis which should be checked before use.

Plots for provenance analysis	The elements involved in the plot[a]	Sources
TFe_2O_3/K_2O-SiO_2/Al_2O_3	**Fe**, K, **Si**, Al	Herron (1988)
SiO_2/Al_2O_3–K_2O/Na_2O	**Si**, Al, K, Na	Bhatia (1983)
$K_2O + Na_2O$–SiO_2	**Si**, K, Na	Roser and Korsch (1986)
F1, F2	**Si**, Ti, Al, Fe, **Mn**, **Mg**, **Ca**, Na, K, **P**	Bhatia (1983)
Co/Th–La/Sc	**Co**, Th, La, Sc	Wronkiewicz and Condie (1987)
Co–Th–Zr	**Co**, Th, Zr	Bhatia and Crook (1986)
Cr/V–Y/Ni	**Cr**, **V**, Y, **Ni**	Mclennan (1993)
TiO_2–Ni	Ti, **Ni**	Floyd et al. (1989)
Ce–La/Yb	**Ce**, La, Yb	Alexander et al. (2000)

[a] Elements identified in bold are considered to have additional components from ancient seawater.

compositional trend interpreted to be due to the provenance difference.

Ternary plots of Al_2O_3–CaO^*+Na_2O–K_2O (A–CN–K) are one of the most commonly used methods for the analysis of weathering, diagenesis, and provenance (Nesbitt and Young, 1984; Young, 1989). CaO^* refers to Ca in silicate. This method traces the weathering trend of feldspar towards clay minerals to retroactively determine the feldspar composition of the source rock. According to the thermodynamic and kinetic processes of feldspar decomposition, plagioclase is weathered in the first stage, resulting in the loss of Na, and Ca, and the weathering trend line is parallel to the A-CN line in the triangular diagram. The weathering of potassium feldspar dominates the second stage, and the trend line is parallel to the A-K line. The determination of CaO^* necessitates the extraction of non-silicate binding Ca from calcite, dolomite, and apatite. However, our compiled data lacks precise information of carbonate and phosphate content for this direct correction. Here, two methods were adopted to calculate CaO^*: i) CaO^* is corrected only for phosphate-bound CaO using P_2O_5. If corrected $CaO^* > Na_2O$, CaO^* is assumed to be equivalent to Na_2O (McLennan, 1993); ii) The enrichment factor of CaO^* is considered equivalent to that of Na_2O if Ca-EF exceeds

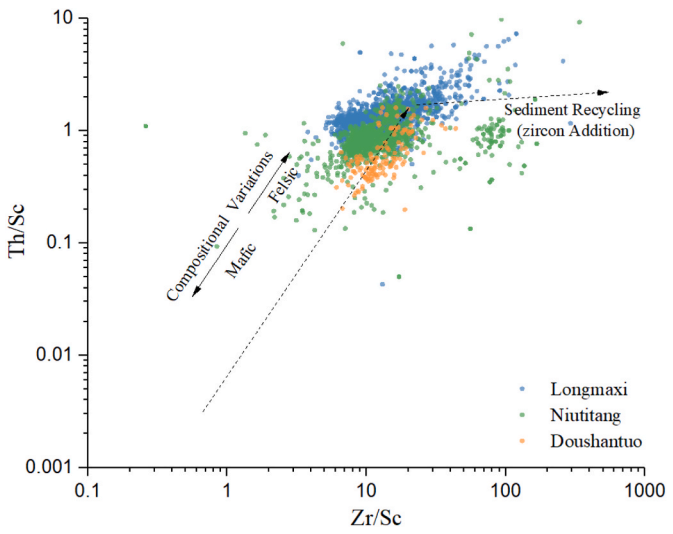

Fig. 6. Th/Sc–Zr/Sc plot showing the influence of sedimentary sorting and recycling on the elemental composition, after (Mclennan, 1993).

those of Na, K, Rb, Sr, and Ba (Garzanti and Resentini, 2016). Samples with an Al_2O_3 content <5% were excluded due to insufficient information on terrestrial debris.

Fig. 7 shows A–CN–K scatter plot of the black shale. The distribution of data points is similar after using two different correction methods for CaO*. The Longmaxi and Niutitang shales shows a clear weathering trend line. When compared with the theoretical trend line, both formations show a tilt towards the K-end element. This indicates a significant influence from diagenetic K-type metasomatism. Additionally, there is a significant difference in the intersection point between its trend line and the CN–K axis. The Niutitang shale has a higher proportion of plagioclase and a lower proportion of potassium feldspar in the source rock compared to the Longmaxi shale. This indicates an increase in the composition of basic magmatic rocks. There is no clear weathering trend line for the Doushantuo shale, and most compositions of the Doushantuo shale are close to the K-end element, indicating strong influence from K-type metasomatism. Therefore, A–CN–K plots are not helpful in the provenance analysis of Doushantuo Shale.

The subsequent provenance analysis relies on a few immobile elements such as Zr, Th, Cr, and Ti, which are generally unaffected by weathering or diagenesis and have shown no significant autogenetic component input based on the previous analysis (Craigie, 2018). However, these elements have a significant positive correlation with Al, indicating the strong influence of the grain-size effect. The stable element ratio is a common method to rule out particle size effects (Craigie, 2018). Here, we combined nine key elemental ratios as provenance proxies including Ti/Th, Th/Sc, Cr/Th, Ti/Zr, Sc/Ta, Ti/Nb, Sc/La, Zr/Sc, and La/Ti. Fig. 8 shows their correlation with Al content. Except for the few dispersion points where the Al_2O_3 content <2.5%, these ratios do not correlate with the Al content, indicating that the grain-size effect has no influence on the effectiveness of these proxies.

4.3. Parent rock composition

Among the immobile elements employed for common provenance analysis, Sc, Ti, Cr, Co, Ni, and V have element contents gradually increasing along with the felsic-intermediate-basic magmatic sequence, whereas La, Th, Zr, and Hf, exhibit the opposite elemental content trend (Hu and Gao, 2007). The pair of elements chosen for the ratio are the two elements with opposite trends to amplify differences in provenance. Among the elements mentioned, Co, Cr, V, and Ni are highly susceptible to changes in marine sedimentary environments. Therefore, when dealing with black shale, it is preferable to use Sc, Ti, La, Th, Zr, and Hf.

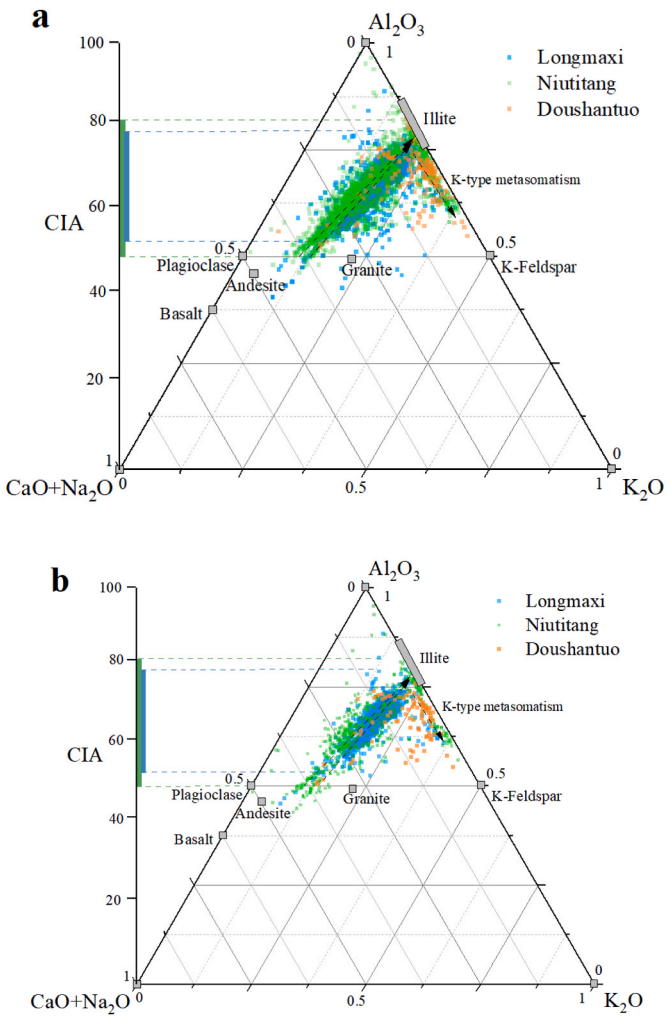

Fig. 7. A–CN–K plot showing the weathering trend and provenance difference of marine black shales (Nesbitt and Young, 1984; Young, 1989). The dashed lines represent the weathering and K-type metasomatism trendlines of the shales. Two different criteria are shown: a) correction method of CaO* from McLennan (1993); b) CaO* was calculated according to Garzanti and Resentini (2016).

The content variation of an element in the magmatic sequence affects its sensitivity in provenance analysis. This variation in Ti, Sc, and Th is far larger than that for La, Zr, and Hf, according to the average elemental content database of magmatic rocks in China (Chi, 2007). The scattered distribution of elemental ratios in Fig. 9 also suggests that the Th/Sc–Ti/Th is superior in discriminating among the three types of black shale. These shales are generally distributed along the trend line of felsic-intermediate-basic magmatic sequences, mainly located within the intermediate-felsic range and gradually extend from intermediate to felsic from the Doushantuo to the Niutitang to the Longmaxi shale. They follow the same trend in the Ti/Zr–Sc/La and Zr/Sc–Ti/La plots, although a few overlapping parts of the scattered elemental ratios exist between these three types of shale. Similar contents of Ta and Nb exist in felsic and basic magmatic rocks, but in intermediate rocks, they are half to two-thirds felsic. Therefore, a significant trend is evident in Fig. 6 among the three types of shale in the Sc/Ta–Ti/Nb plot.

4.4. Tectonic setting of the provenance area

Inferences regarding the tectonic setting may be made based on the composition of the provenance area (Bhatia, 1983). These relationships can be summarized as follows (Condie, 1989): Volcanic activity within

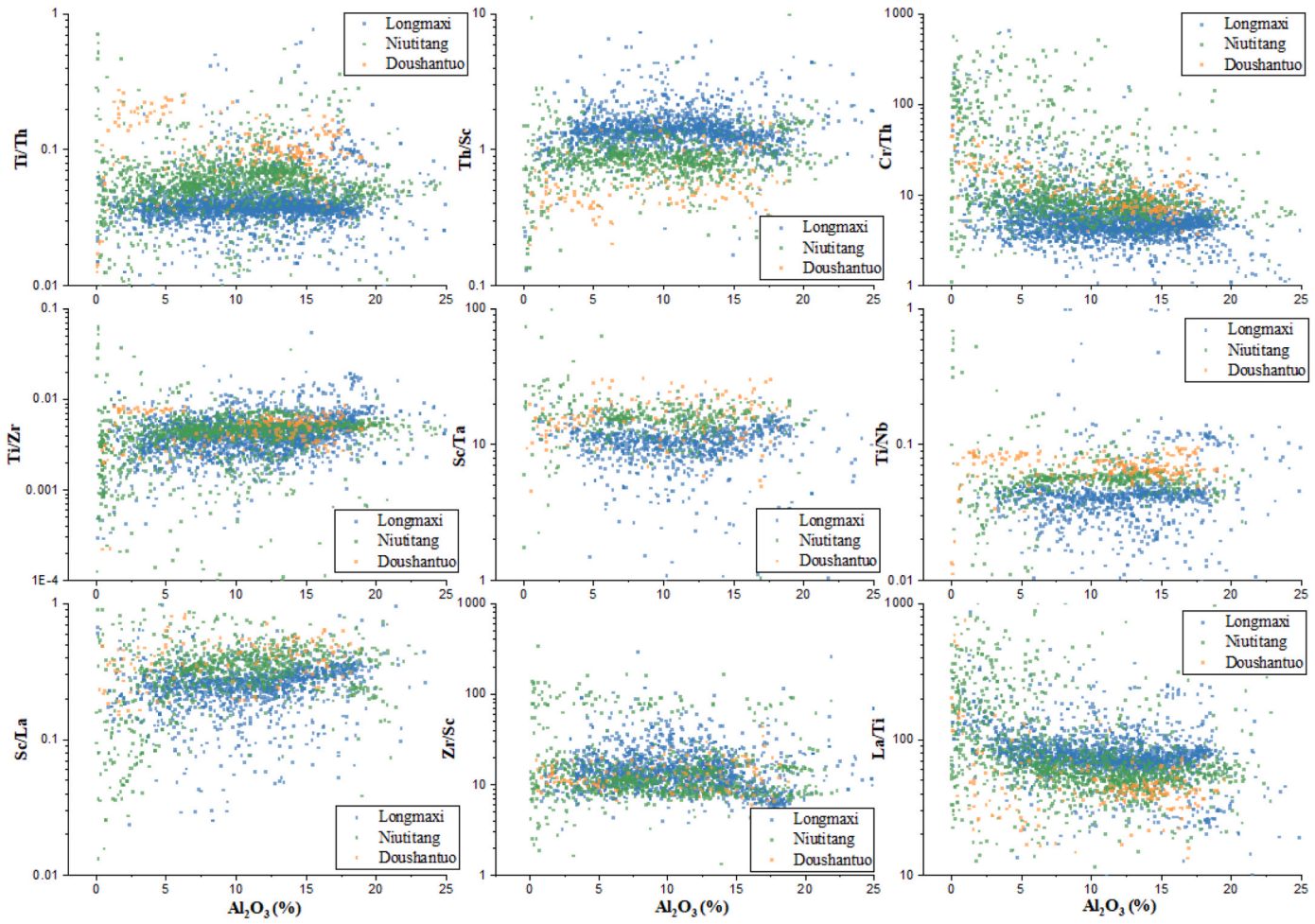

Fig. 8. Correlation between Al content and element ratio proxies in provenance analysis.

continental arcs results mainly in andesite, dacite, and rhyolite, together with small amounts of basalt. Oceanic island arcs form by subduction of the oceanic crust and also reflect a primary composition as a combination of basalt and andesite. However, the primary component of igneous rocks is basalt in the oceanic island arc environment, with reduced amounts of andesite. Conversely, the magmatic products of collisions between continental terranes are commonly granites, including both S-type granites during the collisional stage and A-type granites after the collision. For marine shales deposited on tectonically complex platforms, they may have multiple sets of provenance information superimposed. Therefore, tectonic setting analysis of the provenance area should be combined with the detrital zircon age spectrum.

Paleogeographic analyses spanning the period between sedimentation of the Doushantuo and Niutitang Formations suggest that the Yangtze Platform underwent a deepening of the sea from west to east (Shu et al., 2014). Geological surveys show that clastic rock deposits were formed on the western border of the Yangtze block (Wang et al., 2022), indicating that the sediment during this period primarily originated from the west. The zircon age and Hf isotopes in Ediacaran sediments on the western margin of the Yangtze block indicate that, during this time, the sediment was mainly sourced from local Tonian magmatite (Yao et al., 2022). This period is dominated by intermediate-felsic magmas, supplemented by basic rocks, reflecting an Andean-type continental margin arc environment (Lai and Zhu, 2022). This is consistent with the provenance composition of the Doushantuo shale we defined in the previous section.

The U–Pb age of Cambrian detrital zircons peaks at 730–880 Ma and 530 Ma in the western margin (Yao et al., 2022; Zhang and Xu, 2024). The former peak is similar to that of Ediacara and is related to the Tonian magmatite in the western part of the Yangtze block. The latter peak, corresponding to the Pan African detrital zircon, has characteristics of high automorphic degree and consistent crystallization and sedimentary ages (Chen et al., 2021). The εHf (t) values of the detrital zircon suggest that the magma source primarily comprises recently formed crustal material with some recycled ancient crust. This indicates that the active continental island arc is likely the source of the Pan-African detrital zircon found in the western margin of the Yangtze block (Zhang and Xu, 2024). There is currently a debate about where the Pan African detrital rocks source from. In this period, the Yangtze block is considered to be the northern margin of Gondwana. However, it is uncertain where exactly it links with Gondwana. Possible scenarios include Northern India (Jiang et al., 2003; Cawood et al., 2013), between India and Australia (Xu et al., 2013; Wang et al., 2018), Indochina (Yang et al., 2020), and Arabia (Han et al., 2022). The latest constraint, which is based on the age of zircon and its εHf (t) value, suggests that the Iranian Cadonian arc provided this portion of detrital material towards the western edge of the South China Plate (Han et al., 2022). The Caledonian arc comprises intermediate-felsic magmatic rocks with small amounts of mafic or ultramafic intrusions. These rocks were formed related to continental island arcs resulting from subduction. Recent research has found that there was volcanic activity in the northwest margin of the Yangtze block during the Early Cambrian (530.1 ± 4.3 Ma age), resulting in a thick metamorphic clastic rock volcanic rock series (Wang et al., 2022). The main lithology is sericite quartz schist interbedded with calcareous sandstone, crystalline tuff, and lens-shaped volcanic breccia and conglomerate. The gravel composition of the breccia is

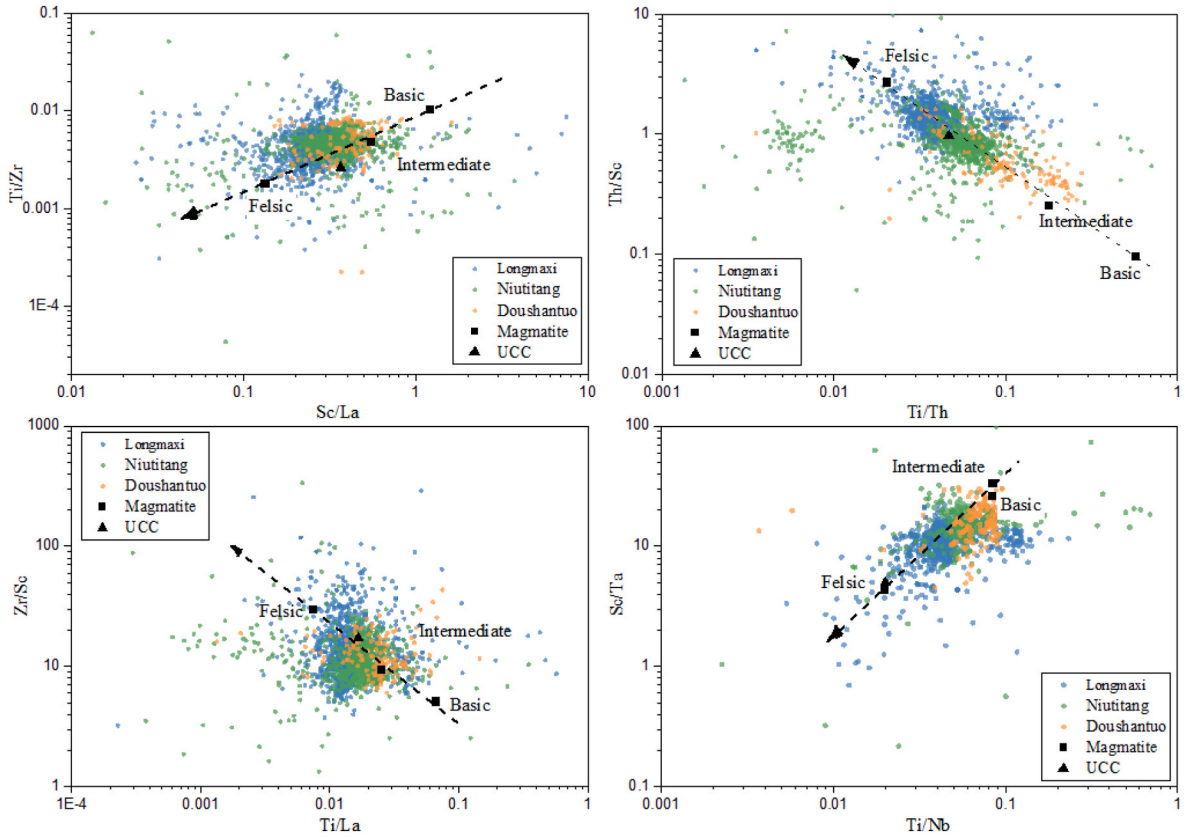

Fig. 9. Scatter plots using trace element ratio for provenance analysis.

complex, mainly including rhyolite, quartz porphyry, limestone, and metamorphic sandstone. This may be a product of tectonic activation and backarc extension after the accretion of the western margin of the Yangtze block, responding to the Pan-African movement (Wang et al., 2022). The compositions of the compiled source elements (previous section) showed an increase in felsic composition from the Doushantuo to the Niutitang Formation. This may correspond to the felsic magma as a terrestrial input from the western edge of the Yangtze block during the Pan-African period. The short transportation distance of zircons (Hofmann et al., 2016) also supports the possibility of the source directly originating from the western Yangtze. To confirm this hypothesis, further independent constraint is needed to interpret the magmatic activity and its geochemical characteristics in the western margin of the Yangtze block.

The U–Pb age of the Longmaxi detrital zircons peak at 447 Ma (Lu et al., 2023). During this period, intracontinental orogeny occurred between the Yangtze and Cathaysia block, with magmatic activity concentrated between 460 and 400 Ma (Xu et al., 2016). Magmatic activity is mainly dominated by peraluminous S-type granite, with a limited distribution of I-type and A-type granites, together with limited intermediate-basic magmatic activity (Zhang and Xu, 2024). This is consistent with the characteristics of the terrestrial elemental composition observed in the Longmaxi Formation shale, where its felsic composition is significantly higher than the other two shales.

Fig. 10 shows the response of the sediment elemental composition to tectonic evolution around the Yangtze plate. The concentrations of Co, Cr, V, Ni, Cu, Zn, and P in intermediate magmatite are 2–7 times higher than those in felsic magmatite as reported by the magmatic geochemical database (Chi, 2007). Therefore, we hypothesize that the amounts of these elements suggest significantly differ terrigenous input in these three periods, matching with the stable elements (Sc, Ti, Th, and La). Although the information on the content of these elements in the shale is

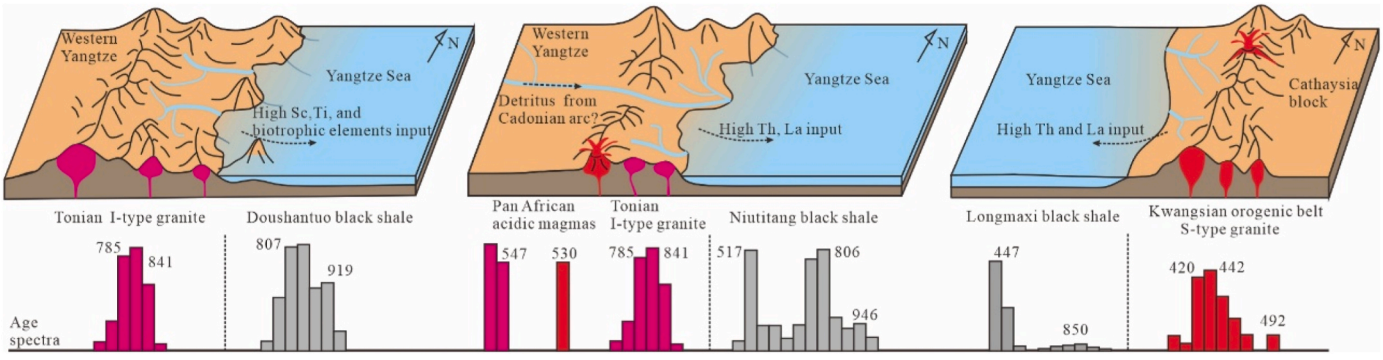

Fig. 10. Schematic showing the provenance composition and evolution of marine black shale in the Yangtze Platform from the Ediacaran to Silurian. Age spectra data from Zhang and Xu (2024), Lu et al. (2023), and Zhang et al. (2013).

overwritten by the strong enrichment of marine autogenetic components, it can be inferred that the terrigenous input of these elements gradually decreased from the Doushantou to the Niutitang to the Longmaxi sedimentary periods. Since most of these elements are biotrophic, the difference in provenance input may have a more profound impact on the paleomarine environment. Large et al. (2015) analyzed the nutrient trace element composition of the palaeo-ocean based on the nutrient elements in marine pyrite. Their results demonstrate the transition from nutrient-rich to nutrient-poor ocean from E-C to O–S. Therefore, continental uplift, erosion, and changes in nutrient flux may serve as primary drivers for oceanic nutrient cycling.

5. Conclusions

We evaluate the provenance composition and infer the evolution of marine black shales in the Yangtze Platform based on a very large database from 307 published papers totaling 12,342 analyzed samples. The black shales of the Longmaxi and Niutitang formations are relatively enriched in redox-sensitive and productivity-related elements such as V, Cr, Mo, U, Co, Ni, Cu, Zn, and Ba. The Doushantuo Formation shows lower contents of these elements and is only significantly enriched in Mo and V. The use of provenance analysis proxies, including V, Mo, Ce, Fe, P, Ba, Cu, Ni, and Si, should be approached with caution due to the potential interference of marine authigenic components. The three black shales have provenance compositions that gradually extend from intermediate to felsic from the Doushantuo to the Niutitang to the Longmaxi Formations based on the trace element ratios plot. The terrigenous input to the three shales has evolved from arc-related magmatite to mainly S-type granites of intracontinental orogeny. These differences in the provenance compositions are a response to the Pan African and Kwangsian orogenic periods which are likely to have impacted the paleomarine environment through the inputs of variable biotrophic elements (Co, Cr, V, Ni, Cu, Zn, and P).

CRediT authorship contribution statement

Xiaoqi Wang: Writing – original draft, Methodology, Investigation, Funding acquisition, Conceptualization. **Mingliang Wang:** Supervision, Funding acquisition. **Derek Elsworth:** Writing – review & editing, Supervision. **TianTian Xu:** Writing – review & editing.

Declaration of competing interest

The authors declare that they have no known competing financial interests or personal relationships that could have appeared to influence the work reported in this paper.

Data availability

I have shared my data in the form of an attachment.

Acknowledgments

This work was supported by the Doctoral Research Initiation Fund of Suzhou University (2021BSK037); the Postdoctoral Research Initiation Fund of Suzhou University (2024BSH004); the Natural Science Foundation of China (Grants 42073059, 42303034, and 42102255); and the Foundation of Suzhou University (Grants 2022AH020084 and 2022AH040210). DE gratefully acknowledges support from the G. Albert Shoemaker endowment.

Appendix A. Supplementary data

Supplementary data to this article can be found online at https://doi.org/10.1016/j.marpetgeo.2024.107003.

References

Aitchison, J., 1982. The statistical analysis of compositional data. J. R. Stat Soc B 44, 139–160.
Alexander, J.L., Bailey, E., Pickering, K., 2000. Using rare earth elements as provenance indicators in mudrocks from a range of tectonic settings. J. Conf. Abstr. 5, 134.
Bhatia, M.R., 1983. Plate tectonics and geochemical composition of sandstones. J. Geol. 91, 611–627.
Bhatia, M.R., Crook, K.A.W., 1986. Trace element characteristics of graywackes and tectonic setting discrimination of sedimentary basins. Contrib. Mineral. Petrol. 92, 181–193.
Caracciolo, L., Von Eynatten, H., Tolosana-Delgado, R., Critelli, S., Manetti, P., Marchev, P., 2012. Petrological, geochemical, and statistical analysis of eocene–oligocene sandstones of the western thrace basin, Greece and Bulgaria. J. Sediment. Res. 82, 482–498.
Cawood, P.A., Wang, Y.J., Xu, Y.J., Zhao, G.C., 2013. Locating South China in rodinia and gondwana: a fragment of greater India lithosphere? Geology 41, 903–906.
Chen, C., Mu, C.L., Zhou, K.K., Liang, W., Ge, X.Y., Wang, X.P., Wang, Q.Y., Zheng, B.S., 2016. The geochemical characteristics and factors controlling the organic matter accumulation of the Late Ordovician-Early Silurian black shale in the Upper Yangtze Basin, South China. Mar. Petrol. Geol. 76, 159–175.
Chen, Q., Zhao, G.C., Sun, M., 2021. Protracted northward drifting of South China during the assembly of Gondwana: constraints from the spatial-temporal provenance comparison of Neoproterozoic-Cambrian strata. Geol. Soc. Am. Bull. 133.
Chi, Q.H., 2007. Handbook of Applied Geochemical Element Abundance Data. Geology Press, Beijing, pp. 140–142.
Condie, K.C., 1989. Origin of the Earth's crust. Global Planet. Change 1, 57–81.
Craigie, N., 2018. Principles of elemental chemostratigraphy. Production of chemostratigraphic correlation schemes. Rudy Swennen. A Practical User Guide 92–96. https://doi.org/10.1007/978-3-319-71216-1.
Ding, M., Li, Y.F., Fan, T.L., Lash, G.G., Wei, X.J., Zhang, T., 2023. Geochemistry of the lower silurian black shales from the upper Yangtze platform, south China: implications for paleoclimate, provenance, and tectonic setting. J. Asian Earth Sci. 242, 105493.
Floyd, P.A., Winchester, J.A., Park, R.G., 1989. Geochemistry and tectonic setting of lewisian clastic metasediments from the early proterozoic loch maree group of gairloch, NW scotland. Precambrian Res. 45, 203–214.
Fralick, P.W., Kronberg, B.I., 1997. Geochemical discrimination of clastic sedimentary rock sources. Sediment. Geol. 113, 111–124.
Garzanti, E., Resentini, A., 2016. Provenance control on chemical indices of weathering (Taiwan river sands). Sediment. Geol. 336, 81–95.
Han, Y.Y., Ran, B., Santosh, M., Luo, C., Liu, S.E., Li, Z.W., Ye, Y.H., Song, J.M., Wang, H., Ding, Y., 2022. Linking South China plate to arabian margin of gondwana: significance for cambrian global plate reconstruction. J. Asian Earth Sci. 237, 105341.
Herron, M.M., 1988. Geochemical classification of terrigenous sands and shales from core or log data. J. Sediment. Res. 58, 820–829.
Hofmann, M.H., Li, X.H., Chen, J., MacKenzie, L.A., Hinman, N.W., 2016. Provenance and temporal constraints of the early cambrian maotianshan shale, yunnan province, China. Gondwana Res. 37, 348–361.
Hu, P.Y., Zhai, Q.G., Wang, J., Tang, Y., Ren, G.M., Zhu, Z.C., Wang, W., Wu, H., 2020. U–Pb zircon geochronology, geochemistry, and Sr–Nd–Hf–O isotopic study of Middle Neoproterozoic magmatic rocks in the Kangdian Rift, South China: slab rollback and backarc extension at the northwestern edge of the Rodinia. Precambrian Res. 347, 105863.
Hu, Z.C., Gao, S., 2007. Upper crustal abundances of trace elements: a revision and update. Chem. Geol. 253, 205–221.
Jiang, G.Q., Sohl, L.E., Christie-Blick, N., 2003. Neoproterozoic stratigraphic comparison of the Lesser Himalaya (India) and Yangtze block (south China): paleogeographic implications. Geology 31, 917–920.
Jiao, W.F., Wu, Y.B., Peng, M., 2009. The oldest basement rock in the Yangtze Craton revealed by zircon U-Pb age and Hf isotope composition. Sci. China Earth Sci. 52, 1393–1399.
Kassambara, A., 2017. Practical Guide to Principal Component Methods in R: PCA, M (CA), FAMD, MFA, HCPC, Factoextra, Sthda.
Lai, S.C., Zhu, Y., 2022. Petrogenesis and geodynamic implications of Neoproterozoic typical intermediate felsic magmatism in the western margin of the Yangtze Block, South China. J. Geomechanics 26, 759–790 (in Chinese with English abstract).
Large, R.R., Halpin, J.A., Lounejeva, E., Danyushevsky, L.V., Maslennikov, V.V., Gregory, D., Sack, P.J., Haines, P.W., Long, J.A., Makoundi, C., 2015. Cycles of nutrient trace elements in the Phanerozoic ocean. Gondwana Res. 28, 1282–1293.
Lê, S., Josse, J., Husson, F., 2008. FactoMineR: an R package for multivariate analysis. J. Stat. Software 25, 1–18.
Li, D.L., Li, R.X., Tan, C.Q., Zhao, D., Xue, T., Zhao, B.S., Khaled, A., Liu, F.T., Xu, F., 2019. Origin of silica, paleoenvironment, and organic matter enrichment in the Lower Paleozoic Niutitang and Longmaxi formations of the northwestern Upper Yangtze Plate: significance for hydrocarbon exploration. Mar. Petrol. Geol. 103, 404–421.
Li, Q., Liu, G.D., Song, Z.Z., Zhang, B.J., Sun, M.L., Tian, X.W., Yang, D.L., Wang, Y.L., Zhu, L.Q., Cao, Y.S., 2022. Organic matter enrichment due to high primary productivity in the deep-water shelf: insights from the lower Cambrian Qiongzhusi shales of the central Sichuan Basin, SW China. J. Asian Earth Sci. 239, 173–189.
Lu, Y.B., Hao, F., Yan, D.T., Lu, Y.C., 2021. Volcanism-induced late boda warming in the late ordovician: evidence from the upper Yangtze platform, south China. Palaeogeogr. Palaeoclimatol. Palaeoecol. 578, 110579.

Lu, Y.B., Yue, Y., Lu, Y.C., Jiang, S., Wang, Y.X., 2023. Sedimentary response to the early silurian (Rhuddanian-Aeronian) post-glacial transgression and kwangsian orogeny in the upper Yangtze region, south China. Palaeogeogr. Palaeoclimatol. Palaeoecol. 623, 111639.
McLennan, Scott, M., 1993. Weathering and global denudation. J. Geol. 101, 295–303.
Mclennan, S.M., 1993. Geochemical approaches to sedimentation, provenance, and tectonics. Geol. Soc. Am. Bull. 84, 21–40.
Nesbitt, H.W., Young, G.M., 1984. Prediction of some weathering trends of plutonic and volcanic rocks based on thermodynamic and kinetic considerations. Geochem. Cosmochim. Acta 48, 1523–1534.
Ravidà, D.C., Caracciolo, L., Heins, W.A., Stollhofen, H., 2023. Towards an improved discrimination and correlation of Permian-Lower Triassic sediments in Central Europe: a chemostratigraphic approach. Sediment. Geol. 452, 106408.
Ren, L.D., Wang, H., 2023. The Pan-African event and its manifestation in the China continent and adjacent regions. Acta Sci. Nat. Univ. Sunyatseni 62, 1–33 (in Chinese with English abstract).
Roser, B.P., Korsch, R.J., 1986. Determination of tectonic setting of sandstone-mudstone suites using SiO_2 content and K_2O/Na_2O ratio. J. Geol. 94, 635–650.
Shu, L.S., 2020. Pre-jurassic tectonics of the South China. Acta. Geol. Sin. 94, 333–360 (in Chinese with English abstract).
Shu, L.S., Jahn, B.M., Charvet, J., Xu, X.S., 2014. Early Paleozoic depositional environment and intraplate tectono-magmatism in the Cathaysia Block (South China): evidence from stratigraphic, structural, geochemical and geochronological investigations. Am. J. Sci. 314, 154–186.
Steiner, M., Wallis, E., Erdtmann, B.D., Zhao, Y.L., Yang, R.D., 2001. Submarine-hydrothermal exhalative ore layers in black shales from South China and associated fossils — insights into a Lower Cambrian facies and bio-evolution. Palaeogeogr. Palaeoclimatol. Palaeoecol. 169, 165–191.
Taylor, S.R., Mclennan, S.M., 1985. The continental crust: its composition and evolution. J. Geol. 94, 57–72.
Wang, W.Z., Zhou, M.F., Zhao, M.F., Zheng, J.H., Lan, J.P., Fan, Z., 2018. Age, provenance and tectonic setting of Neoproterozoic to early Paleozoic sequences in southeastern South China Block: constraints on its linkage to western Australia-East Antarctica. Precambrian Res. 309, 290–308.
Wang, Y.J., Zhang, F.F., Fan, W.M., Zhang, G.W., Chen, S.Y., Cawood, P.A., Zhang, A.M., 2010. Tectonic setting of the South China Block in the early Paleozoic: resolving intracontinental and ocean closure models from detrital zircon U-Pb geochronology. Tectonics 29, 213–254.
Wang, Z.J., Wang, Q.Y., Yang, F., Xiong, G.Q., Ma, L., Du, Q.D., Zheng, B.S., 2022. Study on the deposition and filling process of the Mianyang Changning cratonic rift: implication for the pan-African orogeny on the western margin of Yangtze Block. Sediment. Geol. Tethyan Geol. 42, 350–367 (in Chinese with English abstract).
Wronkiewicz, D.J., Condie, K.C., 1987. Geochemistry of archean shales from the witwatersrand supergroup, South Africa: source-area weathering and provenance. Geochem. Cosmochim. Acta 51, 2401–2416.
Xiao, D., Cao, J., Luo, B., Tan, X.C., Xiao, W.Y., He, Y., Li, K.Y., 2021. Neoproterozoic postglacial paleoenvironment and hydrocarbon potential: a review and new insights from the Doushantuo Formation Sichuan Basin, China. Earth Sci. Rev. 212, 103453.
Xiao, W.Y., Cao, J., Luo, B., He, Y., Zhou, G., Zuo, Z.X., Xiao, D., Hu, K., 2020. Marinoan glacial aftermath in South China: paleo-environmental evolution and organic carbon accumulation in the Doushantuo shales. Chem. Geol. 555, 119838.
Xu, Y.J., Cawood, P.A., Du, Y.S., 2016. Intraplate orogenesis in response to gondwana assembly: kwangsian orogeny, south China. Am. J. Sci. 316, 329–362.
Xu, Y.J., Cawood, P.A., Du, Y.S., Hu, L.S., Yu, W.C., Zhu, Y.H., Li, W.C., 2013. Linking south China to northern Australia and India on the margin of Gondwana: constraints from detrital zircon U-Pb and Hf isotopes in Cambrian strata. Tectonics 32, 1547–1558.
Xue, E.K., Wang, W., Zhou, M.F., Pandit, M.K., Huang, S.F., Lu, G.M., 2021. Late Neoproterozoic-early Paleozoic basin evolution in the Cathaysia Block, South China: implications of spatio-temporal provenance changes on the paleogeographic reconstructions in supercontinent cycles. Geol. Soc. Am. Bull. 133, 717–739.
Yan, D.T., Chen, D.Z., Wang, Z.Z., Li, J., Yang, X.R., Zhang, B., 2019. Climatic and oceanic controlled deposition of late ordovician-early silurian black shales on the north Yangtze platform, south China. Mar. Petrol. Geol. 110, 112–121.
Yan, D.T., Li, S.J., Fu, H.J., Jasper, D.M., Zhou, S.D., Yang, X.R., Zhang, B., Mangi, H.N., 2021. Mineralogy and geochemistry of lower silurian black shales from the Yangtze platform, south China. Int. J. Coal Geol. 237, 103706.
Yang, C., Xian, H.L., Zheng, X.L., Zhu, M.Y., Lu, K., 2020. Provenance evolution of age calibrated strata reveals when and how South China Block collided with Gondwana. Geophys. Res. Lett. 47, e2020GL090282.
Yao, W.H., Li, Z.X., 2016. Tectonostratigraphic history of the ediacaran–silurian Nanhua foreland basin in south China. Tectonophysics 674, 31–51.
Yao, W.H., Zhu, X.Y., Wang, J., Zhou, X.L., Spencer, C.J., Wang, Z.J., Li, Z.X., 2022. Position of South China and Indochina along northern gondwana margin during the ediacaran–silurian period. Precambrian Res. 379, 106809.
Ye, Y.P., Tang, S.H., Xi, Z.D., Jiang, D.X., Duan, Y., 2022. Quartz types in the Wufeng-Longmaxi Formations in southern China: implications for porosity evolution and shale brittleness. Mar. Petrol. Geol. 137, 105479.
Young, H.W.N.M., 1989. Formation and diagenesis of weathering profiles. J. Geol. 97, 129–147.
Zan, B.W., Mou, C.L., Lash, G.G., Ge, X.Y., Wang, X.P., Wang, Q.Y., Yan, J.X., Chen, F.F., Jin, B., 2021. An integrated study of the petrographic and geochemical characteristics of organic-rich deposits of the Wufeng and Longmaxi formations, western Hubei Province, South China: insights into the co-evolution of paleoenvironment and organic matter accumulation. Mar. Petrol. Geol. 132, 105193.
Zhang, G.J., Chen, D.Z., Huang, K.J., Liu, M., Fu, Y., 2021. Dramatic attenuation of continental weathering during the Ediacaran-Cambrian transition: implications for the climatic-oceanic-biological co-evolution. Global Planet. Change 203, 103518.
Zhang, G.W., Guo, A.L., Wang, Y.J., Li, S.Z., Dong, Y.P., Liu, S.F., He, D.F., Cheng, S.Y., Lu, R.K., Yao, A.P., 2013. Tectonics of South China continent and its implications. Sci. China Earth Sci. 43, 1553–1582.
Zhang, J., Xu, Y.J., 2024. Is strike-slip convergence the cause of movement in South China and Guangxi? Acta Sedimentol. Sin. 12, 1–20 (in Chinese).
Zhou, X.L., Liu, Y., Cao, H.Y., Zhong, H.T., Li, Y.C., 2021. Responses of oceanic chemistry to climatic perturbations during the Ordovician-Silurian transition: implications for geochemical proxies and organic accumulations. Mar. Petrol. Geol. 134, 105341.